RESEARCH ARTICLE SUMMARY

PLANT SCIENCE

Synthetic glycolate metabolism pathways stimulate crop growth and productivity in the field

Paul F. South, Amanda P. Cavanagh, Helen W. Liu, Donald R. Ort*

INTRODUCTION: Meeting food demands for the growing global human population requires improving crop productivity, and large gains are possible through enhancing photosynthetic efficiency. Photosynthesis requires the carboxylation of ribulose-1,5-bisphosphate (RuBP) by ribulose-1,5-bisphosphate carboxylase-oxygenase (RuBisCO), but photorespiration occurs in most plants such as soybean, rice, and wheat (known as C_3 crops) when RuBisCO oxygenates RuBP instead, requiring costly processing of toxic byproducts such as glycolate. Photorespiration can reduce C_3 crop photosynthetic efficiency by 20 to 50%. Although various strategies exist for lowering the costs of photorespiration, chamber- and greenhouse-grown plants with altered photorespiratory pathways within the chloroplast have shown promising results, including increased photosynthetic rates and plant size.

RATIONALE: To determine if alternative photorespiratory pathways could effectively improve C_3 field crop productivity, we tested the performance of three alternative photorespiratory pathways in field-grown tobacco. One pathway used five genes from the *Escherichia coli* glycolate oxidation pathway; a second pathway used glycolate oxidase and malate synthase from plants and catalase from *E. coli*; and the third pathway used plant malate synthase and a green algal glycolate dehydrogenase. All enzymes in the alternative pathway designs were directed to the chloroplast. RNA interference (RNAi) was also used to down-regulate a native chloroplast glycolate transporter in the photorespiratory pathway, thereby limiting metabolite flux through the native pathway. The three pathways were introduced with and without the transporter RNAi construct into tobacco, which is an ideal model field crop because it is easily transformed, has a short life cycle, produces large quantities of seed, and develops a robust canopy similar to that of other field crops.

ON OUR WEBSITE

Read the full article at http://dx.doi.org/10.1126/science.aat9077

RESULTS: Using a synthetic biology approach to vary promoter gene combinations, we generated a total of 17 construct designs of the three pathways with and without the transporter RNAi construct. Initial screens for photoprotection by alternative pathway function under high–photorespiratory stress conditions identified three to five independent transformants of each design for further analysis. Gene and protein expression analyses confirmed expression of the introduced genes and suppression of the native transporter in RNAi plants. In greenhouse screens, pathway 1 increased biomass by nearly 13%. Pathway 2 showed no benefit compared to wild type. Introduction of pathway 3 increased biomass by 18% without RNAi and 24% with RNAi, which were consistent with changes in photorespiratory metabolism and higher photosynthetic rates. Ultimately, field testing across two different growing seasons showed >25% increase in biomass of pathway 3 plants compared to wild type, and with RNAi productivity increased by >40%. In addition, this pathway increased the light-use efficiency of photosynthesis by 17% in the field.

CONCLUSION: Engineering more efficient photorespiratory pathways into tobacco while inhibiting the native pathway markedly increased both photosynthetic efficiency and vegetative biomass. We are optimistic that similar gains may be achieved and translated into increased yield in C_3 grain crops because photorespiration is common to all C_3 plants and higher photosynthetic rates under elevated CO_2, which suppresses photorespiration and increases harvestable yield in C_3 crops. ■

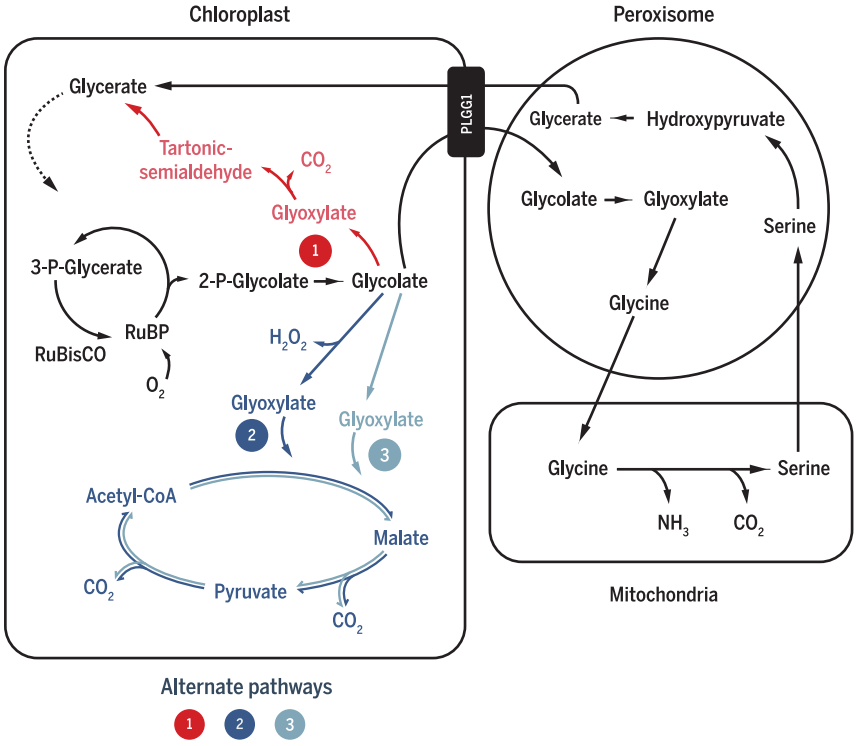

Alternative photorespiratory pathways in tobacco. Three alternative pathways [1 (red), 2 (dark blue), and 3(light blue)] introduced into tobacco chloroplasts for more efficient recycling of glycolate. RNAi suppresses the native glycolate/glycerate transporter PLGG1 to prevent glycolate from leaving the chloroplast and entering the native pathway (gray).

The list of author affiliations is available in the full article online.
*Corresponding author. Email: d-ort@illinois.edu

Cite this article as P. F. South *et al.*, *Science* **363**, eaat9077 (2019). DOI: 10.1126/science.aat9077

RESEARCH ARTICLE

PLANT SCIENCE

Synthetic glycolate metabolism pathways stimulate crop growth and productivity in the field

Paul F. South[1,2], Amanda P. Cavanagh[2], Helen W. Liu[3]*, Donald R. Ort[1,2,3,4]†

Photorespiration is required in C_3 plants to metabolize toxic glycolate formed when ribulose-1,5-bisphosphate carboxylase-oxygenase oxygenates rather than carboxylates ribulose-1,5-bisphosphate. Depending on growing temperatures, photorespiration can reduce yields by 20 to 50% in C_3 crops. Inspired by earlier work, we installed into tobacco chloroplasts synthetic glycolate metabolic pathways that are thought to be more efficient than the native pathway. Flux through the synthetic pathways was maximized by inhibiting glycolate export from the chloroplast. The synthetic pathways tested improved photosynthetic quantum yield by 20%. Numerous homozygous transgenic lines increased biomass productivity by >40% in replicated field trials. These results show that engineering alternative glycolate metabolic pathways into crop chloroplasts while inhibiting glycolate export into the native pathway can drive increases in C_3 crop yield under agricultural field conditions.

Population growth, increasing global affluence, and an expanding bioeconomy are conspiring to increase mid-century agricultural demand by 60 to 120% over 2005 levels, a challenge that current rates of crop productivity improvement averaging <2% per year cannot meet (*1*–*3*). In the 45 years after 1960, global crop productivity increased 135% from 1.84 to 3.96 metric tons per hectare (*4*). The increased use of pesticides, fertilizers and irrigation, and mechanization, along with the adoption of higher-yielding crop varieties that drove this remarkable global increase in productivity, are now largely optimized for major crops and are unlikely to generate sufficient yield increases to meet mid-century agricultural demand. However, photosynthetic efficiency remains standing as a determinant of yield potential with the improvement capacity to double crop productivity (*1*–*3*, *5*, *6*). In C_3 crops such as wheat, rice, and soybeans, photorespiration reduces the photosynthetic conversion efficiency of light into biomass by 20 to 50%, with the largest losses occurring in hot dry climates where yield increases are sorely needed. Whereas ribulose-1,5-bisphosphate carboxylase-oxygenase (RuBisCO) carboxylates ribulose-1,5-bisphosphate (RuBP) during photosynthesis, the unproductive and energy-intensive process of photorespiration results from oxygenation of RuBP by BuBisCO, which becomes more prevalent at higher temperatures and under drought conditions (*6*, *7*). Toxic by-products of the BuBisCO oxygenation reaction (2-phosphoglycolate and glycolate) and of the glycine decarboxylation reaction (ammonia) are recycled by photorespiration into nontoxic products but at the expense of energy and net loss of fixed carbon (*6*, *7*). Some photosynthetic algae, bacteria, and plants have evolved mechanisms to reduce the oxygenation reaction by BuBisCO via carbon-concentrating mechanisms (CCMs), including C_4 photosynthesis (*8*, *9*), inspiring efforts to introduce CCMs into C_3 plants (*8*–*12*). Here we have taken an alternative approach of introducing non-native and synthetic metabolic pathways to recycle the products of BuBisCO oxygenation more efficiently (*13*). Previously, two alternative photorespiratory pathways implemented in *Arabidopsis* improved photosynthesis and plant size in chamber and greenhouse experiments (*14*, *15*). These results inspired us to optimize these alternative photorespiratory pathways in tobacco, a useful agricultural model crop, for field trials. Computer modeling of these alternative pathways revealed the importance of optimized expression of non-native genes to achieve maximum flux through the alternative pathway and thus maximize the benefits for crop plants under field conditions (*16*). Additionally, we sought to minimize flux through the native photorespiratory pathway and maximize flux through the introduced pathways by inhibiting glycolate export from the chloroplast.

[1]Global Change and Photosynthesis Research Unit, United States Department of Agriculture–Agricultural Research Service, Urbana, IL 61801, USA. [2]Carl R. Woese Institute for Genomic Biology, University of Illinois, Urbana, IL 61801, USA. [3]Department of Crop Sciences, University of Illinois, Urbana, IL 61801, USA. [4]Department of Plant Biology, University of Illinois, Urbana, IL 61801, USA.
*Present address: Department of Plant and Microbial Biology, University of California, Berkeley, CA 94720, USA.
†Corresponding author. Email: d-ort@illinois.edu

Results

Transgene assembly

We transformed *Nicotiana tabacum* cv. Petite Havana (tobacco) with three different photorespiratory alternative pathway (AP) designs, expressing as many as seven genes in single constructs (Fig. 1A and table S1). Tobacco is an ideal model crop for these studies because of its completely sequenced genome, short life cycle (3 months from seed to seed), well established high-efficiency transformation protocols, and the ability to form a fully closed canopy like other crops in the field. The AP1 construct targets the five genes of the *Escherichia coli* glycolate oxidation pathway to the chloroplast (Fig. 1A) (*14*). AP2 includes *Arabidopsis* glycolate oxidase (GO) and *Cucurbita maxima* (pumpkin) malate synthase (MS), along with a catalase (CAT) from *E. coli* (Fig. 1A) (*15*). AP3 also contains *C. maxima* MS sequence but replaces the plant GO used in AP2 with *Chlamydomonas reinhardtii* glycolate dehydrogenase (CrGDH) to avoid hydrogen peroxide production when glycolate is converted to glyoxylate (Fig. 1A). With this modification, expression of *E. coli* CAT in the chloroplast is unnecessary (*17*). Using multigene constructs assembled from modular parts by Golden Gate cloning, we generated multiple promoter gene combinations and within-construct position effects to optimize AP performance. We generated five iterations of AP1, three iterations of AP2, and a single design of AP3 for testing (table S1). In addition to the expression of the AP genes, we designed a long hairpin RNA interference (RNAi) construct and added it to the library of multigene constructs to reduce the expression of the chloroplast glycolate-glycerate transporter *PLGG1* with the goal of minimizing glycolate flux out of the chloroplast and into the native pathway (Fig. 1 and table S1) (*18*, *19*). In total, we successfully transformed 17 different constructs of the three AP designs into tobacco with and without the inclusion of an RNAi module targeting the PLGG1 transporter.

Gene and protein analysis confirm chloroplast-localized transgene expression

Transgene expression analysis conducted on three independent transformants of each AP design selected for further analysis confirmed strong expression of the transgenes along with ~80% RNAi suppression of *PLGG1* expression (Fig. 1B and fig. S1). Immunoblot analysis of whole-cell extract was normalized on the basis of total protein content and verified using antibodies against the RuBisCO large subunit and actin (fig. S2). Immunoblot analysis of isolated intact chloroplasts from AP3 plants (Fig. 1C) verified that the construct design of AP3 directs CrGDH and MS protein to the chloroplast and that RNAi suppresses expression of the PLGG1 transporter protein. The cytoplasmic marker protein actin was undetectable in the isolated chloroplast fraction, ensuring that the AP3 proteins in the chloroplast fraction was not a result of cytoplasmic contamination (Fig. 1C). Moreover, the chloroplast marker PGL35 was only faintly detectable in the whole-leaf extracts but was greatly enriched in the isolated chloroplast fraction (Fig. 1C). Whereas MS was also greatly enriched in the

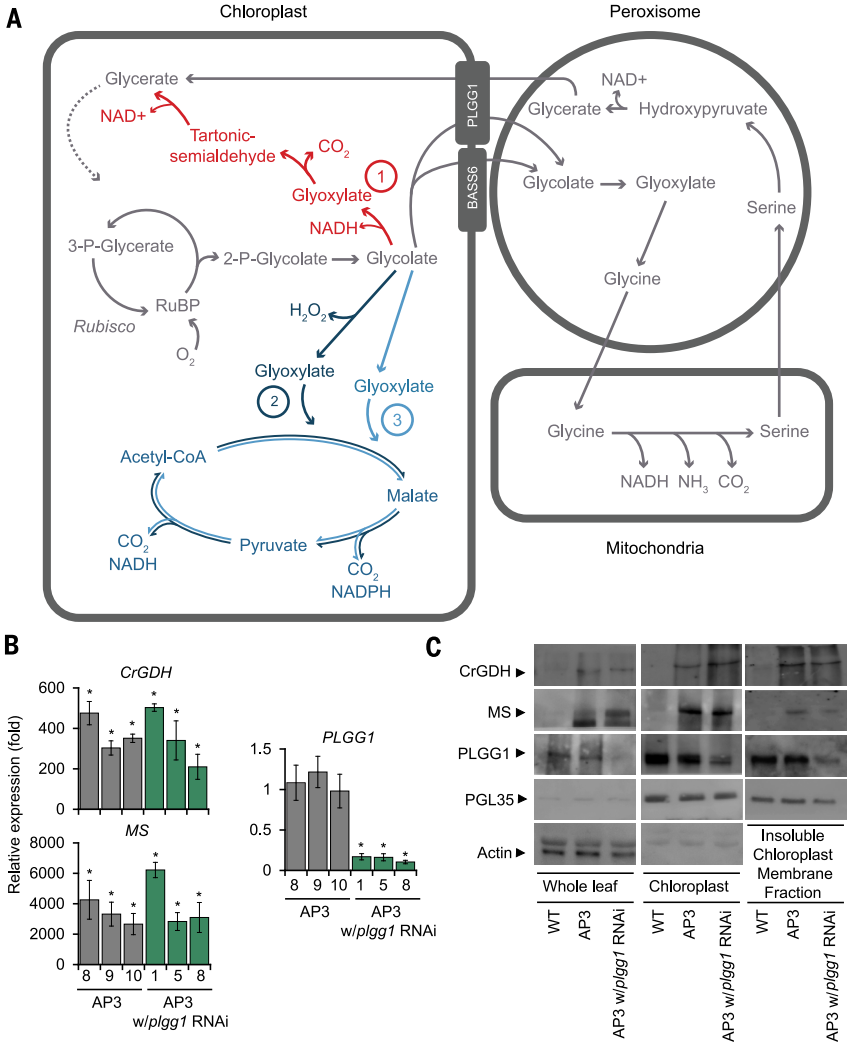

Fig. 1. Alternative photorespiratory pathways. (**A**) Model of three alternative photorespiration pathway designs. AP1 (red) converts glycolate to glycerate using five genes from the *E. coli* glycolate pathway encoding the enzymes glycolate dehydrogenase, glyoxylate carboligase, and tartonic semialdehyde reductase. AP2 (dark blue) requires three introduced genes encoding glycolate oxidase, malate synthase, and catalase (to remove hydrogen peroxide generated by glycolate oxidase). AP3 (blue) relies on two introduced genes: *Chlamydomonas reinhardtii* glycolate dehydrogenase and *Cucurbita maxima* malate synthase. (**B**) qRT-PCR analysis of the two transgenes in AP3 and the target gene *PLGG1* of the RNAi construct. Results for three independent transformation events are shown with (1, 5, and 8) and without (8, 9, and 10) *PLGG1* RNAi. Error bars indicate SEM. * indicates statistical difference at $P < 0.05$ compared to WT based on one-way ANOVA. Actual *P* values are shown in supplementary data set 15. (**C**) Immunoblot analysis from whole leaves and isolated chloroplasts, including the insoluble membrane fraction, using custom antibodies raised against the indicated target genes, cytosolic marker actin, and chloroplast-specific marker platoglobulin 35 (PGL35). Five micrograms of protein was loaded per lane. Arrows indicate detected protein based on molecular weight. The kinetic properties of CrGDH, as well as numerous malate synthase enzymes, have been previously characterized (table S3) (*17*).

chloroplast fraction, CrGDH appeared to be much less enriched in this fraction (Fig. 1C). Glycolate dehydrogenases have be shown to strongly associated with membranes in both chlorophytes and bacteria (*20*, *21*) and thus may have been inefficiently extracted from our chloroplast preparation (*17*). Isolation of the insoluble membrane fraction from the chloroplast extraction showed that a large fraction CrGDH in tobacco chloroplasts was associated with the membranes (Fig. 1C) and that CrGDH was enriched relative to PGL35 in the membrane fraction.

AP plants are resistant to photorespiration stress

Following selection for construct expression by selectable marker screening [BASTA resistance (bar) gene added to all constructs] (table S1) and genotyping selection for single-insert homozygous transgenic plants, all independent constructs of the three AP designs were assessed for resistance to photorespiration stress in a high-throughput chlorophyll fluorescence assay. Photorespiratory mutants typically display impaired growth and photosynthesis when transferred from elevated CO_2 concentrations ($[CO_2]$) to ambient air, which is accompanied by the onset of photoinhibition that can be diagnosed by monitoring chlorophyll fluorescence (*19*, *22*–*24*). We hypothesized that AP function would be photoprotective under high photorespiratory stress, thus protecting photosystem II operating efficiency (i.e., Fv′/Fm′) from photodamage (*19*, *22*). Previously, this method of monitoring Fv′/Fm′ after illumination in low $[CO_2]$ enabled identification of photorespiration mutants that cause photoinhibition (*19*, *22*, *24*). Using this protocol to monitor AP function, we exposed thousands of single-insert homozygous T2 seedling plants to 24 hours of high light intensity (1200 μmol m^{-2} s^{-1}) and very low $[CO_2]$ (1 to 38 μbar CO_2) and then compared Fv′/Fm′ in the transformants with azygous wild-type (WT) and empty vector (EV) controls (fig. S3). Many independent transformants (66% of AP1, 54% of AP2, and 84% of AP3 plants) were significantly more photoprotective under this severe photorespiratory stress. Versions of AP1 and AP3 sustained 33 to 48% higher Fv′/Fm′ values compared to WT and EV controls (Fig. 2, A and B, and data set S1). Under ambient $[CO_2]$, there were no observed differences in Fv′/Fm′ between the AP and control lines. However, *PLGG1* RNAi inhibition of glycolate efflux from the chloroplast reduced Fv′/Fm′ when these plants were shifted from elevated $[CO_2]$ to ambient (fig. S4). This photoinhibited phenotype of the *PLGG1* RNAi plants was not only rescued by transgenic complementation with AP1 or AP3 constructs, but was also substantially more resistant to photoinhibition than WT and EV controls (Fig. 2C and dataset S1).

AP plants show enhanced biomass accumulation in greenhouse growth studies

Following the initial photoprotection screen and expression analysis, we determined the impact of the three APs on plant growth in greenhouse growth studies. Both the AP1 and AP3 designs significantly increased dry-weight biomass relative to the WT plants. Overall, AP1 plants increased dry weight biomass by 13%, but the benefit was lost when the *PLGG1* RNAi module was present (Fig. 3B). AP2 introduction did not significantly alter dry weight (Fig. 3B). Three AP3 lines that sustained much higher Fv′/Fm′ values (200-8,9,10) compared to WT and EV were taller (Fig. 3A) and showed the largest increases in biomass in greenhouse studies, with a 24% increase with and 18% increase without the *PLGG1* RNAi module compared to WT (Fig. 3B). We also tested an AP3 line that had the same Fv′/Fm′ as WT and EV (200-4), which showed no increase in biomass, and one line that had an intermediate Fv′/Fm′ (200-6) that showed a small but statistically significant biomass increase in greenhouse studies (fig. S5, A and C). Transcript expression analysis of AP3

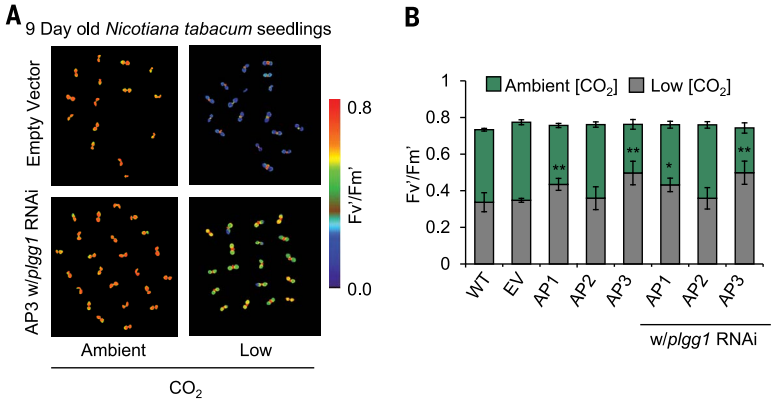

Fig. 2. AP plant lines are more photoprotective under photorespiration stress. (**A**) Representative photos of 9-day-old T2 transgenic tobacco lines during the chlorophyll fluorescence photoprotection screen for AP pathway function showing AP3 protecting photosystem II from photodamage under severe photorespiratory conditions. (**B**) Combined values of the three AP construct designs with and without RNAi targeting the glycolate-glycerate transporter PLGG1. Error bars indicate SEM. * indicates statistical difference compared to WT based on one-way ANOVA at $P \leq 0.05$, ** $P \leq 0.001$. Fv′/Fm′ for individual lines is described in supplementary data set 1. Actual significant P values are shown in supplementary data set 15.

events 200-4 and 200-6 revealed that CrGDH and MS expression was greatly reduced compared to transgenic events 200-8,9,10 (fig. S5B).

AP3 plants have an altered photorespiratory metabolite profile

We further investigated the AP3 plants that showed the greatest growth stimulation and gene expression to determine the effect of AP3 enzymes on the leaf photorespiratory metabolite profile. We performed gas chromatography followed by mass spectrometry on leaf samples from greenhouse-grown WT and AP3 plants to analyze the photorespiratory intermediates glycolate, glyoxylate, glycine, and serine and the AP3-specific intermediate pyruvate (Fig. 4). AP3 introduction with and without the RNAi module increased glyoxylate and pyruvate concentration compared to WT, suggesting altered native photorespiration and possibly flux through the alternative pathway (Fig. 4, B and F). AP3 plants with and without the RNAi module also had decreased concentrations of the photorespiratory intermediates serine, for which photorespiration is a major source (*25*), and glycerate, possibly due to a diversion of carbon away from the native photorespiratory pathway (Fig. 4, D and E). Glycine concentrations were similar in AP3 and WT plants (Fig. 4C). AP3 with the RNAi module targeting the glycolate-glycerate transporter *PLGG1* had increased glycolate accumulation compared to WT in a manner similar to the *Arabidopsis* T-DNA insertion mutant *plgg1-1* (Fig. 4A) (*18*, *19*).

AP3 plants exhibit increased photosynthetic rate and chloroplast [CO_2]

To test if altered photorespiration due to introduction of the AP3 design in plants affects rates of photosynthesis, we compared CO_2 assimilation rates (A) as a function of intercellular CO_2 concentrations (C_i) under saturating light in AP3 and WT plants. AP3 plant lines with and without the *PLGG1* RNAi module had increased rates of photosynthesis compared to WT (Fig. 5A). Modeling of the A/C_i curves showed increases in the maximum rate of BuBisCO carboxylation (V_{cmax}) visualized in the initial slope of the A/C_i curve in AP3 lines (Fig. 5, A and C). We observed no statistical differences in the maximum rate of electron transport (J_{max}) in any AP design (fig. S6). Increases in V_{cmax}, which is a property of BuBisCO enzymatic activity, could be due to increased BuBisCO protein content or increased availability of CO_2 as a substrate for BuBisCO. Immunoblot analysis shows no difference in BuBisCO content on a per microgram protein basis (fig. S2), suggesting that the observed difference is based on increased availability of CO_2 at the site of carboxylation in the chloroplast. Increases in CO_2 availability for BuBisCO carboxylation could arise from increased mesophyll conductance (g_m; i.e., the diffusion of CO_2 into mesophyll cell chloroplasts) or from the direct release of photorespiratory CO_2 in the chloroplast by the decarboxylation of malate and pyruvate in the plastid (Fig. 1A), both of which would result in observed increase in V_{cmax} determined from A/C_i curves (*26*). There is no apparent reason to expect that the introduction of these alternative pathways would decrease the resistance for the movement of CO_2 from the mesophyll intercellular air space to the

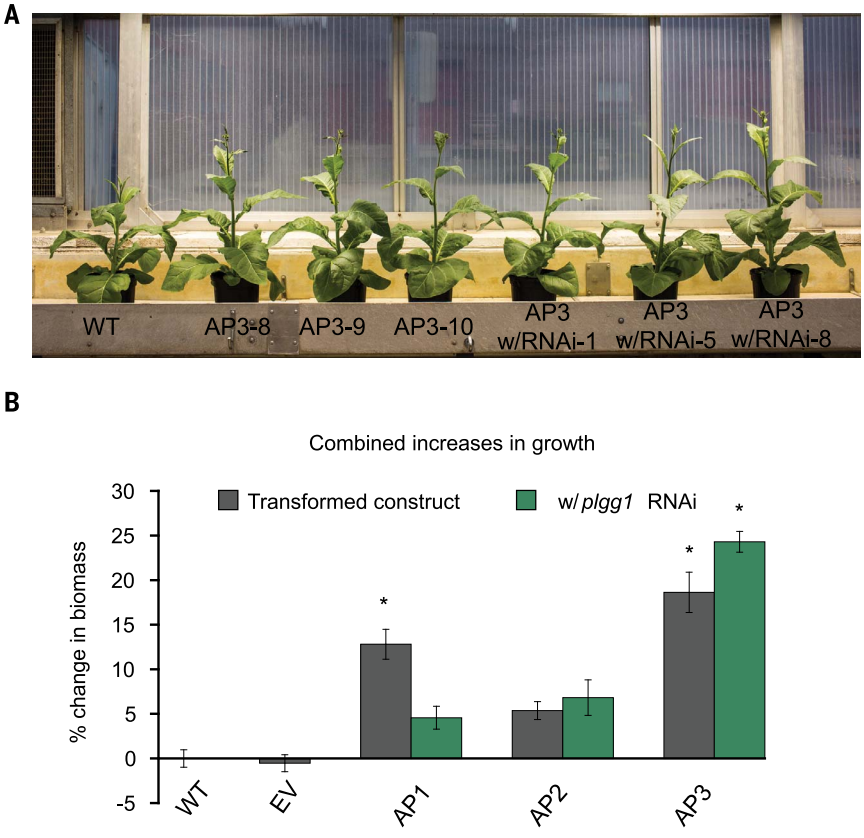

Fig. 3. Photorespiration AP lines increase biomass under greenhouse conditions. (**A**) Photos of 6-week-old AP3 and WT plants grown in the greenhouse. Individual plant lines are indicated in the labels below the plant. (**B**) Percent difference in total dry weight biomass of the indicated combined plant lines. * indicate statistical difference based on one-way ANOVA. Error bars are SEM, $n = 7$ (plants measured), $P < 0.05$ values listed in data set 15.

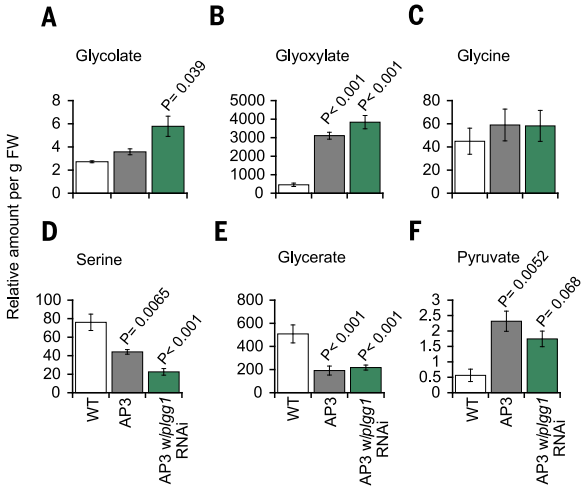

Fig. 4. Photorespiratory and AP3 metabolic intermediates. (**A** to **F**) Relative amount of the indicated metabolite detected from ~40 mg of leaf tissue (fresh weight; FW) sampled in the late morning. Metabolite concentrations were reported as concentrations relative to the internal standard, which is the target compound peak area divided by peak area of hentriacontanoic acid: N_i (relative concentration) = X_i (target compound peak area) * X^{-1}IS (peak area of hentriacontanoic acid) per gram fresh weight. Error bars indicate SEM, n = 4 leaf samples. Statistical differences between AP3 designs and WT based on one-way ANOVA, with P values indicated. All P values are listed in dataset 15.

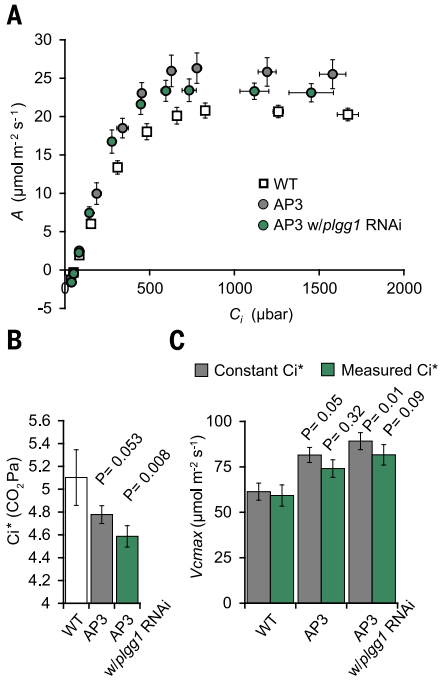

Fig. 5. Photosynthetic efficiency of greenhouse-grown plants. Data are the combined result of three independent transformants (hereafter referred to as combined) with and without *PLGG1* RNAi. (**A**) CO_2 assimilation based on intercellular [CO_2] (C_i). (**B**) Combined apparent CO_2 compensation point: C_i* calculated using the common intercept method and slope regression (*29*). (**C**) Combined maximum rate of BuBisCO carboxylation (V_{cmax}). V_{cmax} values are presented at 25°C and modeled from photosynthetic response under changing CO_2 concentration. Gray bars indicate constant C_i*; green bars indicate derived values based on measured C_i*. Error bars indicate SEM. P values for statistical comparison to WT based on one-way ANOVA are given.

chloroplast stroma or from the mitochondria to the chloroplast stroma. However, an increase in g_m contributing to increased CO_2 availability within the AP3 plant chloroplast is difficult to rule out, largely because modeling of g_m requires knowledge of, or assumptions about, the conductance of CO_2 released from the mitochondria during the conversion of glycine to serine to the chloroplast, which is directly affected by the introduction of the alternative pathway.

Theory predicts that the release of photorespiratory CO_2 in the chloroplast by the AP pathways, instead of in the mitochondria through the native photorespiratory pathway, would lower C_i*, the intercellular [CO_2] at which the chloroplast [CO_2] reaches Γ*, the [CO_2] in the chloroplast at which the rates of BuBisCO oxygenation and carboxylation are equal (*27*–*29*). To determine C_i*, we measured the internal [CO_2] at which CO_2 response curves measured at different subsaturating illumination intensities intersect (*29*). AP3 plants with the RNAi module targeting *PLGG1* showed a significant reduction of 10% in C_i* and AP3 plants without the RNAi module showed a significant reduction of 6.4% in C_i* compared to WT (Fig. 5B). The observed decreases in C_i*, coupled with unaltered respiration (fig. S7), are consistent with elevated chloroplastic [CO_2] due to decarboxylation of malate and pyruvate within the introduced pathway (Figs. 1A and 5B and fig. S6), which would also explain the significantly higher values of V_{cmax} in AP3 plants compared to WT plants (Fig. 5, A and C, and fig. S6). Accounting for the observed C_i* in A/C_i curve analysis reduces the apparent change in V_{cmax} further indicating that the difference in V_{cmax} was not due to changes in BuBisCO content or activity but rather by increased chloroplastic [CO_2] (Fig. 5C).

AP plants show increased photosynthetic rates, quantum efficiency, and biomass accumulation in replicated field trials

In the 2016 growing season, we tested four independent events of AP1, two independent events of AP2, and five independent transformation events of AP3, along with two WT and two EV controls in the field, using a randomized single block design experiment (fig. S8). Biomass increased by 16% in AP1 lines and 10% in one of the AP2 lines tested (fig. S9). The three AP3 lines that showed the largest biomass increases in the greenhouse consistently showed the largest increases in dry-weight biomass, with total biomass increasing by as much as 23% relative to WT (fig. S9). Independent AP3 events 200-4 and 200-6, in which CrGDH and MS expression was significantly lower compared to other transgenic events (fig. S5B) and showed less or no improvement in greenhouse biomass (fig. S5C), also showed no increases in total biomass in the 2016 field season (fig. S9). We anticipated, owing to their lower energetic requirements, that the AP pathways would improve the maximum quantum efficiency of net CO_2 assimilation (Φa) relative to the native pathway. Φa increased in lines of all AP pathways, in many cases by >20%, including those containing the RNAi module targeting the PLGG1 transporter (fig. S10) but not in AP3 events 200-4 and 200-6 (fig. S11A). The high–biomass-producing AP3 plant lines exhibited an increased light-saturated rate of assimilation compared to WT, to several AP1 lines, and to all AP2 plant lines (fig. S10C) and to AP3 events 200-4 and 200-6 (fig. S11).

To validate the 2016 field results and improve the statistical power of comparisons with AP3 plants under agricultural conditions, we tested five randomized replicate blocks of three AP3 independent transformed lines with and without the RNAi module targeting *PLGG1* in comparison to WT during the 2017 growing season (fig. S12). The AP3 plant lines showed a 25% increase in total dry-weight biomass (22% leaf, 44% stem), and the inclusion of the *PLGG1* RNAi module in AP3 designs further increased leaf dry biomass to 33%, stem dry biomass to 50%, and total dry biomass to 41% compared to WT (Fig. 6A). That AP3 plant lines with the RNAi module showed a significant leaf and total dry weight biomass increase (12% and 17%, respectively) over the AP3-only plants supports our hypothesis that forcing greater glycolate flux through the synthetic pathway by inhibiting flux through the native photorespiratory pathway drove the increased productivity. Total mid-day starch content in AP3 plants increased by ~70% and in AP3 with *PLGG1* RNAi by ~40% compared to the WT control (Fig. 6B). The apparent quantum

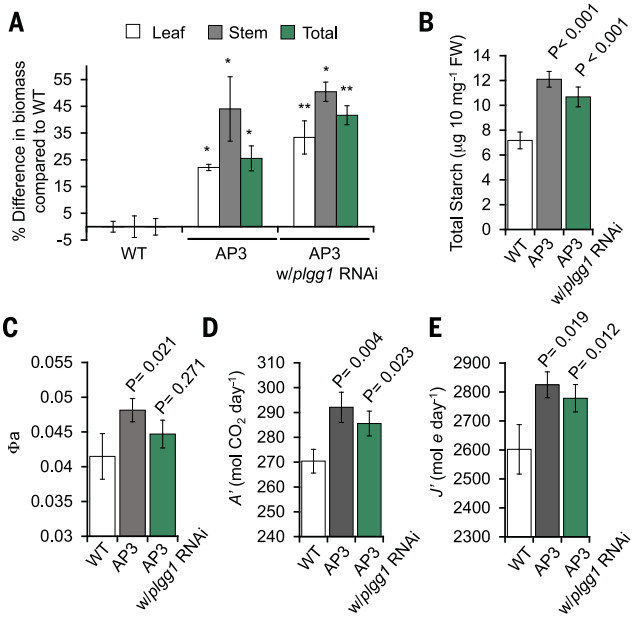

Fig. 6. Plant productivity and photosynthetic performance in 2017 field trials. (**A**) Percent difference from WT for stem, leaf, and total biomass of AP3 with and without the *PLGG1* RNAi module. Data are the combined result of three independent transformants with and without *PLGG1* RNAi. * indicates significance compared to WT and ** indicates significance between WT and AP3-only lines compared to AP3 with RNAi lines. *P* values are shown in supplementary data set 15. (**B**) Total combined accumulated leaf starch for indicated lines extracted from 10 mg of fresh weight leaf material. (**C**) Combined apparent quantum efficiency of photosynthesis (Φa) determined by linear regression of assimilation based on available light-response curves. (**D**) Combined accumulated assimilation of CO_2 (*A′*) based on diurnal analysis of photosynthesis. (**E**) Combined accumulated electrons used in electron transport determined from assimilation based on diurnal photosynthesis. Error bars indicate SD, and *P* values are indicated based on two-way ANOVA.

efficiency of photosynthesis increased in both AP3 plant pathways; by 7% with and 17% without *PLGG1* RNAi for the 2017 field season (Fig. 6C and fig. S13). Because plants with both AP3 designs exhibited increases in the quantum efficiency of photosynthesis and decreases in C_i*, we hypothesized that total daily net carbon gain through photosynthesis would be higher compared to WT, resulting in the observed increases in biomass over the growing season (Figs. 5B and 6, A and C). Indeed, modeled daily net carbon gain from measurements of photosynthesis over a diurnal time course in plants containing AP3 showed an increase of 5 to 8% in CO_2 assimilation (*A′*) and increases in electron use in photosynthesis (*J′*) compared to WT (Fig. 6, D and E).

Discussion

We showed that installing synthetic glycolate metabolic pathways into tobacco chloroplasts drove large increases in biomass accumulation in both greenhouse conditions and in the field under agricultural conditions. Because AP3 plants exhibited the greatest growth stimulation, we selected this pathway for more in-depth characterization. In summary, the AP3 transgene products CrGDH and MS localized to the chloroplast (Fig. 1C). Evidence that these transgene products function in the chloroplast to catalyze the reactions depicted in Fig. 1 include the stimulation of the rate of photosynthesis (Fig. 5) and improvement of photosynthetic quantum yield (Fig. 6 and fig. S10), the lowering of C_i* (Fig. 5) and increase in the initial slope of an A/C_i relationship (Fig. 5) that both indicate increased [CO_2] in the chloroplast, and the altered photorespiratory metabolite profile (Fig. 4). In addition, the direct role of this pathway in chloroplast glycolate metabolism is supported by its ability to prevent photoinhibition and rescue the reduced growth phenotype of *PLGG1* RNAi tobacco lines (fig. S4). Moreover, AP3 lines that contain the full transgene construct but with reduced transgene expression showed less, or no improvement in greenhouse (fig. S5C) or field biomass (fig. S9), and Φa values similar to WT (fig. S11) provide evidence that the amount of expression of the introduced alternative photorespiratory pathway drove the extent of improved growth and increased photosynthetic efficiency.

Of the two alternative pathways to photorespiration that inspired our designs (*13*, *14*), AP2 showed limited improvements in plant productivity, and 24% of the independent transgenic AP2 lines resulted in stunted growth and yellow leaves (fig. S14C). The AP1 design improved productivity in tobacco, but the enhancement associated with AP1 was eliminated in both greenhouse and field settings when the *PLGG1* RNAi module was added (Fig. 3 and fig. S9). Modeling (*16*) predicted that directing the complete flux of glycolate through the AP1 pathway by inhibiting glycolate export from the chloroplast would result in the largest increase in energy savings, photosynthetic efficiency, and growth among all designs. Elimination of the AP1 enhancements by the *PLGG1* RNAi module implies that this introduced pathway may not have had sufficient kinetic capacity to handle the full glycolate flux under high rates of BuBisCO oxygenation. Further optimization of expression of AP1 genes and/or use of AP1 genes of different origins and kinetic properties may lead to achieving the full benefits that modeling predicts for this design. The AP3 design containing *C. maxima* MS and CrGDH reliably increased plant biomass and improved photosynthetic efficiency (Figs. 3, 5, and 6), and the phenotype is dependent on the level of expression of the transgenes in the independent transformation events (fig. S5). The inclusion of an RNAi module to reduce expression of the *PLGG1* chloroplast glycolate-glycerate transporter in numerous independent transformant plant lines increased postharvest dry-weight biomass compared to AP3 introduction alone by 17% ($P < 0.001$) (Figs. 3 and 6A and fig. S13). Without an alternative photorespiration pathway in place, inhibition of *PLGG1* expression by RNAi decreased plant growth and led to photoinhibition (i.e., reduced Fv′/Fm′) when these plants were transferred from elevated [CO_2] to ambient air (fig. S4), as was reported previously for the *plgg1-1* T-DNA knockout line in *Arabidopsis* (*23*). Thus, the genetic complementation of the low-growth photoinhibited phenotype and the significant increase in biomass in AP3 lines with RNAi over AP3 alone are consistent with the expected benefit of directing a greater proportion of the glycolate flux through the synthetic pathway in the chloroplast and away from the native photorespiratory pathway outside of the chloroplast (*18*, *19*). Indeed, forcing greater glycolate flux through the synthetic pathway by inhibiting glycolate transport out of the chloroplast through PLGG1 into the native photorespiratory pathway resulted in growth stimulation in field trials of >40% for the AP3 plants with RNAi. The glycolate-glycerate exchange transporter PLGG1 works in tandem with a second glycolate exporter BASS6 to stoichiometrically balance the export of two glycolate molecules with the import of one glycerate molecule during photorespiration (*18*). Thus, targeting the expression of both transporters may further test AP3 kinetic capacity and may drive even greater growth stimulation. Recognizing that these alternative pathways are intervening in the central metabolism of photosynthetic cells, it will be important to validate the biochemistry that is occurring as AP pathway intermediates may well have destinations that are different from those depicted in Fig. 1A.

Although inhibiting photorespiration under normal oxygen-containing atmospheres invariably results in inhibited photosynthesis and growth (*7*), some evidence indicates that stimulating

photorespiratory flux can enhance photosynthetic rate and plant growth. Overexpression of the H-protein in the glycine decarboxylase complex or overexpression of plant glycolate oxidase (GO) can lead to increased photosynthesis and biomass production (*30*, *31*). In both of these reports, the overexpression of these photorespiration genes was accompanied by an increase in stomatal conductance that itself would be expected to increase photosynthesis and growth under water-replete conditions. Conversely, four different photorespiration mutants (*pglp1, shm1, hpr1,* and *glyk1*) partially lost stomatal responsiveness to altered CO_2 availability, possibly indicating that alternative pathways could influence plant adaptation through stomatal signaling (*32*). We saw no statistical differences in stomatal conductance (fig. S15, A and B) or the expression of GO (fig. S15C) in AP3 tobacco plants, indicating that neither of these contributed to the stimulations observed in AP3 plant lines. Whether the installation of these alternative pathways may affect global changes in the transcriptome and the proteome and if that may have secondary impacts on plant growth outside of changes to primary metabolism remain to be determined. Energy demand calculations suggest that AP3 would consume more adenosine 5′-triphosphate than native photorespiration, similar to AP2 (*33*). It is likely that CrGDH uses the electron transport chain as an electron acceptor (*17*), and the decarboxylation of malate and pyruvate generate reducing equivalents (Fig. 1). However, the global effect of AP3 and *PLGG1* repression on energy balance, as well as the possible fate of intermediates from AP3 in sucrose synthesis or the tricarboxylic acid cycle, will need to be assessed (*17*, *33*).

Tobacco was selected for these proof-of-concept experiments not only for its ease of genetic transformation but also because it is an ideal model crop that is robust in the field, forms a fully closed canopy, and produces large quantities of seed, circumventing the need for numerous seed amplification generations, further accelerating the timeline to field testing. The photorespiratory mechanism is common to all C_3 plants, although energetic costs and yield reductions depend on species-specific kinetic properties of BuBisCO, as well as the temperature and $[CO_2]$ under which the crop is growing. Previous work has demonstrated that alternative photorespiration pathways show a benefit to crop plants *Camelina sativa* (*34*) and potato (*35*) in greenhouse and chamber experiments, but it remains to be seen whether the increase in vegetative biomass that we observed in tobacco with AP3 in the field can be translated into increased seed or tuber production in crops such as soybean, cowpea, and potato. In greenhouse studies, only one AP3 line containing the *PLGG1* RNAi module showed a significant increase in total seed weight (fig. S13E), but seed is not a major sink in tobacco as it is in grain crops. However, because increased photosynthetic efficiency due to the suppression of photorespiration in C_3 crops grown in elevated $[CO_2]$ results in increased seed yield (*5*, *36*), we are optimistic that use of alternative metabolic pathways to photorespiration will also lead to increases in seed yield. Indeed, in this work, the observed stimulation of whole-plant biomass production was much larger than the stimulation of photosynthesis on a leaf area basis (5 to 8% increase in CO_2 assimilation resulting in 25 to 41% increase in dry-weight biomass; compare Fig. 6A with Fig. 6, D and E), showing the benefit of compound interest from creating greater leaf area earlier in the growth cycle.

Materials and Methods

Plant genetic transformation

Nicotiana tabacum cv. Petite Havana was genetically transformed using *Agrobacterium tumefaciens* strain C58C1-mediated transformation (*37*). The 17 binary plasmids used in this study were assembled as described and listed in table S1 (*19*). AP1 genes originated from *E. coli (14)*. AP2 genes originated from *Arabidopsis thaliana* (glycolate oxidase) and *Cucurbita maxima* (malate synthase) and *E. coli* (catalase) sources as described (*15*, *38*). AP3 genes originated from *Chlamydomonas reinhardtii* for glycolate dehydrogenase and as described for AP2 for *C. maxima* malate synthase (*15*, *17*). Targeting to the chloroplast was designed by the addition of either the *Arabidopsis* BuBisCO small subunit (RbcS) or phosphoglucomutase transit peptide sequence added to the N terminus of the gene constructs. The RNAi module that targets the plastidic glycolate-glycerate transporter *PLGG1* was designed using 300 base pairs of exon sequence derived from the Sol genomics network (https://solgenomics.net). All binary plasmids contained the BASTA resistance (*bar*) gene as a selectable marker for plant transformation. A minimum of 10 independent T_0 transformations were generated to produce T_1 progeny. T-DNA copy number was determined on T_1 plants through quantitative reverse transcription–quantitative polymerase chain reaction (qRT-PCR) analysis (iDNA Genetics, Norwich UK) (dataset 17) (*39*). From these results, a minimum of five independent transformation events were selected to self and produce T_2 progeny. Copy-number analysis was repeated to verify single insert homozygous lines for each transformation event. Non-single insert lines were not further characterized (for a representative timeline of characterization of AP3 lines see dataset 20). All WT controls used in this study were azygous plants, which have been through the transformation protocol but lost the construct including the selectable marker resistance during segregation.

Chlorophyll fluorescence measurements

Tobacco T_2 seeds were germinated under ambient air conditions on Murashige and Skoog (MS) plates with essential vitamins in a controlled environment chamber (Environmental Growth Chambers, Chagrin Falls, Ohio, USA) with 14 hours day (25°C)/10 hours night (22°C) and light intensity of 500 μmol m^{-2} s^{-1}. Eight days after germination, seedling plates were transferred to a custom assembled low-$[CO_2]$ chamber inside the controlled environment growth chamber (fig. S1). The light levels were increased to 1200 μmol m^{-2} s^{-1} for 24 hours and $[CO_2]$ was maintained below 38 μbar (fig. S1). For *PLGG1* RNAi-only plants, which have strongly depressed photorespiratory capacity, T_1 lines were germinated on soil under elevated $[CO_2]$ conditions for 9 days and transferred to ambient air for 3 days prior to screening. Fv′/Fm′ was determined on each plate using the CF Imager Technologica (http://www.technologica.co.uk/). Maximum flash intensity was 6800 μmol m^{-2} s^{-1} for 800 ms. Image values were obtained for each individual plant by detecting colonies within the fluorimager software program defining each position as described (*19*, *22*, *40*).

Gene expression and protein detection

Plants were grown under greenhouse or field conditions as described below. Five leaf discs were harvested from three plants per line (2.9 cm^2, ~100 mg). RNA and protein were extracted from the same leaf samples using the NucleoSpin RNA/Protein kit (Macherey-Nagel GmbH & Co.KG, Düren, Germany). cDNA was generated from extracted RNA using the Quantinova reverse transcriptase kit (QIAGEN, USA). A minimum of three biological replicates, including three technical replicates each, were performed for all samples. Gene expression was analyzed using a Bio-Rad CFX connect real-time PCR system (Bio-Rad Laboratories, USA). Relative changes in transcript levels were determined using the ΔΔCt method with primers directed toward the transgene transcripts and the *L25* gene as a standard control gene (*41*). cDNA was amplified using a SSO advanced SYBR green master mix (Bio-Rad), and primer sequences are described in table S2.

Total protein from AP3 was extracted using the Nucleospin protein/RNA kit described above or from frozen leaf material ground in liquid nitrogen, resuspended in lysis buffer [50 mM HEPES (pH 7.6), 300 mM sucrose, 2 mM $MgCl_2$] plus plant protease inhibitor cocktail (Sigma-Aldrich). Protein was quantified using the protein quantification assay (Macherey-Nagel GmbH & Co. KG, Düren, Germany). Unless indicated otherwise, 5 μg of protein was loaded per lane and separated by 10% SDS–polyacrylamide electrophoresis (SDS-PAGE). PAGE gels were transferred to polyvinylidene difluoride (PVDF) membranes (Immobilon-P, Millipore, USA) using a Bio-Rad semi-dry transfer system or the Bio-Rad Trans-Blot turbo system. After blocking in a 6% milk TBS solution, membranes were incubated with custom antibodies raised against the malate synthase (MS) and PLGG1 (Agrisera, Vännäs, Sweden) and glycolate dehydrogenase (GDH) (Genscript, USA). As a protein loading control, antibodies raised against the large subunit of BuBisCO (RbcL) and actin were used (Agrisera, Vännäs, Sweden). After subsequent washing and incubation with anti-rabbit secondary antibody (Bio-Rad, USA), chemiluminescence was detected with the Image-Quant LAS4010 scanner (GE Healthcare Life Sciences, Pittsburgh, USA).

Chloroplasts were isolated in a manner similar to that described (*19*), with tobacco-specific

modifications following (42). Leaf tissue was collected from 6-week-old WT and AP3 plants, briefly homogenized in extraction buffer [50 mM MES-NaOH (pH 6.1), 0.33 M sorbitol, 2 mM EDTA, 2 mM $MgCl_2$, 1 mM $MnCl_2$, 20 mM NaCl, 2 mM isoascorbic acid, and 1% polyvinypyrrolidone-40], filtered through three layers of Miracloth (Calbiochem), and centrifuged at 4°C for 4 min at 2500*g* to pellet chloroplasts. Pelleted chloroplasts were resuspended in 5 ml of buffer [50 mM HEPES-NaOH (pH 6.8), 0.33 M sorbitol, 2 mM EDTA, 2 mM $MgCl_2$, 1 mM $MnCl_2$, 5 mM isoascorbic acid, 1 mM sodium pyrophosphate, 5 mM glutathione] using a fine paintbrush, applied to a 20-ml Percoll density gradient [top to bottom: 40% (v/v) and 90% (v/v) Percoll in resuspension buffer], and centrifuged at 4°C for 30 min at 2500*g*. Intact chloroplasts accumulated at the 40 to 90% interface and were removed by aspiration, washed twice in 10 volumes of resuspension buffer, and collected by centrifugation for 10 min at 2500 g.

Plastid proteins were extracted by lysing the chloroplasts in a hypotonic buffer [10 mM Tricine-NaOH (pH 8.0), 1% (v/v) plant protease inhibitor cocktail (Sigma-Aldrich), and 5 mM dithiothreitol (DTT)], followed by two freeze-thaw cycles. Insoluble membrane fractions from the chloroplast isolation were isolated by centrifugation at 10,000 g for 5 min. The pellet was resuspended in 2× SDS sample buffer plus 10% DTT, then briefly sonicated. The membrane fraction proteins were then precipitated using ice-cold acetone. After centrifugation (10,000 g for 5 min), the acetone was removed, and the pellet was air dried. The protein pellet was then resuspended in SDS sample buffer plus 10% DTT. Protein concentration was then determined using a total protein quantification kit (Macherey-Nagel GmbH & Co.KG, Düren, Germany).

Photorespiratory metabolite analysis

Metabolite analysis was performed as described (19). Briefly, ~40 μg of fresh leaf tissue was harvested from 6-week-old greenhouse-grown plants taken late morning (~10:00 to 11:00 a.m.) and flash frozen in liquid nitrogen. Leaf material was crushed using a genogrinder (Biospec products) and extracted in 100% ice-cold methanol. Samples were then submitted to the Metabolomics Center, Roy J. Carver Biotechnology Center, University of Illinois at Urbana-Champaign and processed as described (19). All known artificial peaks were identified and removed. To allow comparison among samples, all data were normalized to the internal standard in each chromatogram and the sample fresh weight. The spectra of all chromatogram peaks were evaluated using the AMDIS 2.71 program (NIST). Metabolite concentrations were reported as concentrations relative to the internal standard, which was the target compound peak area divided by peak area of hentriacontanoic acid: N_i (relative concentration) = X_i (target compound peak area) * X^{-1}IS (peak area of hentriacontanoic acid) per gram fresh weight. The instrument variability was within the standard acceptance limit of 5%.

Growth analysis (greenhouse)

Homozygous single-insert T_2 seeds were germinated on LC1 Sunshine mix (Sun Gro 202 Horticulture, Agawam, MA, USA). Ten days after germination, seedlings were transferred to 4L pots (400C, Hummert International, Earth City, MO, USA) with LC1 Sunshine mix supplemented with slow-release fertilizer (Osmocote Plus 15/9/12, The Scotts Company LLC, Marysville, OH, USA). Pots were randomized within the greenhouse and positions were changed before each watering approximately every 4 to 5 days. Greenhouse growth conditions are tabulated in supplementary dataset 12. Aboveground biomass was harvested and dried for 2 weeks to attain constant weight, and dry weights determined for stem and leaf fractions. Stem fractions included reproductive material developed at time of final harvest.

Field experiments

In 2016, five independent transformation events of AP3, four events of AP1, and two independent transformations of AP2, with two wild type (WT) and two empty vector (EV) controls, were planted in a randomized single block design. Homozygous single-insert T_2 seeds were germinated in pots containing soil mix (Sun Gro 202 Horticulture, Agawam, MA, USA) on 14 May 2016 and grown for 7 days before transferal to floating trays as described (43). Plants were transplanted at the University of Illinois Energy Farm field station (40.11°N, 88.21°W, Urbana, IL, USA) on 6 June 2016 after the field was prepared as described (43). Each plot consisted of 6 × 6 plants spaced 30 cm apart (fig. S8). The internal 16 plants per plot were the indicated transgenic plant lines surrounded by a border of 20 WT plants. An additional two-row border of WT plants surrounded the full experiment that consisted of 26 plots. Watering was provided as needed from six water towers placed within the experiment. Weather data, including light intensity, air temperature, and precipitation, were measured for the 2016 field season as described (43) (supplementary data set 13).

Apparent quantum efficiency of photosynthesis (Φa) and the light-saturated rate of photosynthetic CO_2 assimilation at ambient (400 μbar) and low (100 μbar) [CO_2] were measured on the youngest fully expanded leaf 14 to 20 days after transplanting in the field. Φa was determined from assimilation measurements in response to light levels at the indicated [CO_2]. Gas exchange measurements were performed using Li-Cor 6400XT instruments with a 2-cm^2 fluorescence measuring cuvette for which chamber leaks were corrected as outlined in the manual (LI-COR Biosciences, Lincoln, NE, USA). Measurements of CO_2 assimilation were conducted at incidental light intensities of 1200, 380, 120, 65, 40, 30, 25, 18, and 10 μmol m^{-2} s^{-1}, and absorbed light was calculated using an integrating sphere (Ocean-Optics, Largo, FL, USA) (23). Assimilation was recorded after a minimum of 120 s at each light level. Φa was calculated from the slope of the initial linear response of CO_2 assimilation at low light levels. The saturating rate of assimilation (A_{sat}) was determined at 1200 μmol m^{-2} s^{-1} light intensity at the indicated [CO_2]. Leaf and stem biomass were determined for 16 plants per plot at 7 weeks post planting. Aboveground biomass was harvested and separated into leaf and stem fractions. Plant material was dried at 65°C to constant weight for a minimum of 2 weeks prior to biomass measurements.

To increase the statistical power of the field experiment, the 2017 growing season focused on six independent transgenic AP3 lines. The field design consisted of five replicate blocks with seven randomized 6 × 6 plants plots per block (fig. S11). The central 16 plants were the AP3 transgenic line or WT surrounded by a WT border. The entire 35 plot-area was surrounded by an additional row of WT as a border. Single-insert homozygous T_2 lines generated from the same harvest time were sown on LC1 Sunshine mix and germinated for 7 days. After 7 days, seedlings were transplanted to floating trays as described above. Fourteen days after transplant to floating trays, plants were transplanted at the Energy Farm field station at the University of Illinois, Urbana, IL, USA, on 21 June 2017. Watering was provided as needed using parallel drip irrigation. Photosynthesis measurements to determine Φa were performed 2 to 5 July, 2017, and Φa was measured as described above. Measurements of CO_2 assimilation in response to light began pre-dawn and were conducted at light intensities of 0, 10, 18, 25, 30, 40, 65, 120, 380, 1200, and 2000 μmol mol^{-1}. Diurnal measurements of photosynthesis were performed starting pre-dawn on 14 July 2017 and measured every 2 hours on two plants per plot per block. Light levels and chamber temperature was set to ambient values based on incoming light levels using a PAR sensor on the Li-Cor 6400XT and a built-in temperature sensor. Reference [CO_2] was maintained at 400 μbar. Diurnal measurements were continued until after dusk. At 49 days post-germination, eight plants per plot were harvested from all five replicate blocks. Aboveground biomass was separated into leaf and stem fractions and dried in a drying oven for 2 weeks to constant weight before biomass measurements. For starch analysis, 10 mg of leaf material was collected on 14 July, frozen in liquid nitrogen, and stored at −80°C. Starch was assayed using the Enzychrom starch assay kit (Bioassay Systems, Hayward, CA, USA). Colorimetric measurements were performed on a Biotek Synergy HT plate reader (Biotek Winooski, VT, USA).

Photosynthetic CO_2 response

Photosynthetic compensation point (C_i*) measurements were performed using a Li-Cor 6800 (Li-Cor Biosciences) equipped with a fluorescence chamber. C_i* was determined using the common intersection method by measuring the CO_2 response of photosynthesis under various subsaturating irradiances (29, 44, 45). The common intersection was determined using slope–intercept regression to produce more accurate and consistent values of C_i* (29). Plants were acclimated under 250 μmol m^{-2} s^{-1} light at 150 μbar CO_2 until

photosynthesis reached steady state and then measured at 150, 120, 90, 70, 50, and 30 μbar CO_2 under light intensities of 250, 165, 120, 80, and 50 μmol m^{-2} s^{-1}. The x-intersection point was converted to C_i* according to (*29*).

To determine the net photosynthetic assimilation rate from a CO_2 dose response, the fifth leaf from the base of 7-week-old *N. tabacum* plants was measured using a Li-Cor 6800 infrared gas analyzer (Li-Cor Biosciences, Lincoln, NE, USA) with leaf temperature controlled at 25°C and light intensity set at 1500 μmol m^{-2} s^{-1}. Leaves were acclimated at a [CO_2] of 400 μbar to achieve a steady-state rate of assimilation. The [CO_2] of the response curve was set at 400, 200, 100, 50, 30, 400, 600, 800, 1000, 1500, 2000 μbar, and measurements were taken when assimilation reached a steady state rate. To determine the maximum rate of carboxylation (V_{cmax}) and maximum electron transport rate (J_{max}), a model for leaf photosynthesis with temperature corrections was used assuming a mesophyll conductance of 0.57 mol^{-2} s^{-1} bar^{-1} (*46*), then adjusted using the determined value of Ci*.

Statistical analysis

All statistical analysis was performed using Origin Pro 2016 (version 9.3.226, Origin Lab Corporation Northampton, MA, USA). For Fv′/Fm′ measurements, each plate contained a minimum of 10 seedlings and the data shown reflect the averaged values. Significance was evaluated by one-way analysis of variance (ANOVA). Relative changes in gene expression were analyzed by one-way ANOVA with three technical replicates per biological replicate from either greenhouse- or field-grown samples. Greenhouse biomass experiments were analyzed by a one-way ANOVA with a minimum of five biological replicates. Biomass data from the 2016 field season were analyzed by a one-way ANVOA with 16 biological replicates. Biomass data from the 2017 field season were analyzed by a two-way ANOVA (genotype × block) with eight biological replicates per genotype per block. Greenhouse photosynthetic measurements were analyzed by a one-way ANOVA, and three biological replicates per measurement and field photosynthetic measurements were analyzed by a two-way ANOVA with two plant replicates per plot and five randomized replicate blocks. All ANOVA testing was followed with a Tukey's post-hoc test for means comparison. ANOVA tables for each analysis are included in supplementary data set 15.

REFERENCES AND NOTES

1. D. K. Ray, N. D. Mueller, P. C. West, J. A. Foley, Yield trends are insufficient to double global crop production by 2050. *PLOS ONE* **8**, e66428 (2013). doi: 10.1371/journal.pone.0066428; pmid: 23840465
2. X. G. Zhu, S. P. Long, D. R. Ort, Improving photosynthetic efficiency for greater yield. *Annu. Rev. Plant Biol.* **61**, 235–261 (2010). doi: 10.1146/annurev-arplant-042809-112206; pmid: 20192734
3. D. R. Ort *et al*., Redesigning photosynthesis to sustainably meet global food and bioenergy demand. *Proc. Natl. Acad. Sci. U.S.A.* **112**, 8529–8536 (2015). doi: 10.1073/pnas.1424031112; pmid: 26124102
4. J. A. Burney, S. J. Davis, D. B. Lobell, Greenhouse gas mitigation by agricultural intensification. *Proc. Natl. Acad. Sci. U.S.A.* **107**, 12052–12057 (2010). doi: 10.1073/pnas.0914216107; pmid: 20551223
5. E. A. Ainsworth, S. P. Long, What have we learned from 15 years of free-air CO_2 enrichment (FACE)? A meta-analytic review of the responses of photosynthesis, canopy properties and plant production to rising CO_2. *New Phytol.* **165**, 351–371 (2005). doi: 10.1111/j.1469-8137.2004.01224.x; pmid: 15720649
6. H. Bauwe, M. Hagemann, A. R. Fernie, Photorespiration: Players, partners and origin. *Trends Plant Sci.* **15**, 330–336 (2010). doi: 10.1016/j.tplants.2010.03.006; pmid: 20403720
7. C. Peterhansel, I. Horst, M. Niessen, C. Blume, R. Kebeish, S. Kürkcüoglu, F. Kreuzaler, Photorespiration. *The Arabidopsis Book*, e0130 (2010).
8. G. D. Price *et al*., The cyanobacterial CCM as a source of genes for improving photosynthetic CO_2 fixation in crop species. *J. Exp. Bot.* **64**, 753–768 (2013). doi: 10.1093/jxb/ers257; pmid: 23028015
9. U. Schlüter, A. P. Weber, The road to C4 photosynthesis: Evolution of a complex trait via intermediary states. *Plant Cell Physiol.* **57**, 881–889 (2016). doi: 10.1093/pcp/pcw009; pmid: 26893471
10. M. Matsuoka, R. T. Furbank, H. Fukayama, M. Miyao, Molecular engineering of C4 photosynthesis. *Annu. Rev. Plant Physiol. Plant Mol. Biol.* **52**, 297–314 (2001). doi: 10.1146/annurev.arplant.52.1.297; pmid: 11337400
11. M. L. Schuler, O. Mantegazza, A. P. Weber, Engineering C4 photosynthesis into C3 chassis in the synthetic biology age. *Plant J.* **87**, 51–65 (2016). doi: 10.1111/tpj.13155; pmid: 26945781
12. B. M. Long, B. D. Rae, V. Rolland, B. Förster, G. D. Price, Cyanobacterial CO_2-concentrating mechanism components: Function and prospects for plant metabolic engineering. *Curr. Opin. Plant Biol.* **31**, 1–8 (2016). doi: 10.1016/j.pbi.2016.03.002; pmid: 26999306
13. M. Betti *et al*., Manipulating photorespiration to increase plant productivity: Recent advances and perspectives for crop improvement. *J. Exp. Bot.* **67**, 2977–2988 (2016). doi: 10.1093/jxb/erw076; pmid: 26951371
14. R. Kebeish *et al*., Chloroplastic photorespiratory bypass increases photosynthesis and biomass production in *Arabidopsis thaliana*. *Nat. Biotechnol.* **25**, 593–599 (2007). doi: 10.1038/nbt1299; pmid: 17435746
15. A. Maier *et al*., Transgenic introduction of a glycolate oxidative cycle into *A. thaliana* chloroplasts leads to growth improvement. *Front. Plant Sci.* **3**, 38 (2012). doi: 10.3389/fpls.2012.00038; pmid: 22639647
16. C. P. Xin, D. Tholen, V. Devloo, X. G. Zhu, The benefits of photorespiratory bypasses: How can they work? *Plant Physiol.* **167**, 574–585 (2015). doi: 10.1104/pp.114.248013; pmid: 25516604
17. M. H. Aboelmy, C. Peterhansel, Enzymatic characterization of *Chlamydomonas reinhardtii* glycolate dehydrogenase and its nearest proteobacterial homologue. *Plant Physiol. Biochem.* **79**, 25–30 (2014). doi: 10.1016/j.plaphy.2014.03.009; pmid: 24681750
18. T. R. Pick *et al*., PLGG1, a plastidic glycolate glycerate transporter, is required for photorespiration and defines a unique class of metabolite transporters. *Proc. Natl. Acad. Sci. U.S.A.* **110**, 3185–3190 (2013). doi: 10.1073/pnas.1215142110; pmid: 23382251
19. P. F. South *et al*., Bile acid sodium symporter BASS6 can transport glycolate and is involved in photorespiratory metabolism in *Arabidopsis thaliana*. *Plant Cell* **29**, 808–823 (2017). doi: 10.1105/tpc.16.00775; pmid: 28351992
20. B. B. Beezley, P. J. Gruber, S. E. Frederick, Cytochemical localization of glycolate dehydrogenase in mitochondria of chlamydomonas. *Plant Physiol.* **58**, 315–319 (1976). doi: 10.1104/pp.58.3.315; pmid: 16659670
21. A.-K. J. Sallal, N. A. Nimer, The intracellular localization of glycolate oxidoreductase in Escherichia coli. *FEBS Lett.* **258**, 277–280 (1989). doi: 10.1016/0014-5793(89)81673-4; pmid: 2689218
22. M. R. Badger, H. Fallahi, S. Kaines, S. Takahashi, Chlorophyll fluorescence screening of *Arabidopsis thaliana* for CO_2 sensitive photorespiration and photoinhibition mutants. *Funct. Plant Biol.* **36**, 867–873 (2009). doi: 10.1071/FP09199
23. B. J. Walker, P. F. South, D. R. Ort, Physiological evidence for plasticity in glycolate/glycerate transport during photorespiration. *Photosynth. Res.* **129**, 93–103 (2016). doi: 10.1007/s11120-016-0277-3; pmid: 27251551
24. S. Takahashi, H. Bauwe, M. Badger, Impairment of the photorespiratory pathway accelerates photoinhibition of photosystem II by suppression of repair but not acceleration of damage processes in Arabidopsis. *Plant Physiol.* **144**, 487–494 (2007). doi: 10.1104/pp.107.097253; pmid: 17400706
25. R. M. Benstein *et al*., Arabidopsis phosphoglycerate dehydrogenase1 of the phosphoserine pathway is essential for development and required for ammonium assimilation and tryptophan biosynthesis. *Plant Cell* **25**, 5011–5029 (2013). doi: 10.1105/tpc.113.118992; pmid: 24368794
26. C. J. Bernacchi, E. L. Singsaas, C. Pimentel, A. R. Portis Jr., S. P. Long, Improved temperature response functions for models of Rubisco-limited photosynthesis. *Plant Cell Environ.* **24**, 253–259 (2001). doi: 10.1111/j.1365-3040.2001.00668.x
27. D. Tholen, G. Ethier, B. Genty, S. Pepin, X. G. Zhu, Variable mesophyll conductance revisited: Theoretical background and experimental implications. *Plant Cell Environ.* **35**, 2087–2103 (2012). doi: 10.1111/j.1365-3040.2012.02538.x; pmid: 22590996
28. B. J. Walker *et al*., Uncertainty in measurements of the photorespiratory CO_2 compensation point and its impact on models of leaf photosynthesis. *Photosynth. Res.* **132**, 245–255 (2017). doi: 10.1007/s11120-017-0369-8; pmid: 28382593
29. B. J. Walker, D. C. Skabelund, F. A. Busch, D. R. Ort, An improved approach for measuring the impact of multiple CO_2 conductances on the apparent photorespiratory CO_2 compensation point through slope-intercept regression. *Plant Cell Environ.* **39**, 1198–1203 (2016). doi: 10.1111/pce.12722; pmid: 27103099
30. L. L. Cui, Y. S. Lu, Y. Li, C. Yang, X. X. Peng, Overexpression of glycolate oxidase confers improved photosynthesis under high light and high temperature in rice. *Front. Plant Sci.* **7**, 1165 (2016). doi: 10.3389/fpls.2016.01165; pmid: 27540387
31. P. E. López-Calcagno *et al*., Overexpressing the H-protein of the glycine cleavage system increases biomass yield in glasshouse and field-grown transgenic tobacco plants. *Plant Biotechnol. J.* 10.1111/pbi.12953 (2018). doi: 10.1111/pbi.12953; pmid: 29851213
32. M. Eisenhut *et al*., Photorespiration is crucial for dynamic response of photosynthetic metabolism and stomatal movement to altered CO_2 availability. *Mol. Plant* **10**, 47–61 (2017). doi: 10.1016/j.molp.2016.09.011; pmid: 27702693
33. C. Peterhansel, C. Blume, S. Offermann, Photorespiratory bypasses: How can they work? *J. Exp. Bot.* **64**, 709–715 (2013). doi: 10.1093/jxb/ers247; pmid: 22996676
34. J. Dalal *et al*., A photorespiratory bypass increases plant growth and seed yield in biofuel crop *Camelina sativa*. *Biotechnol. Biofuels* **8**, 175 (2015). doi: 10.1186/s13068-015-0357-1; pmid: 26516348
35. G. Nölke, M. Houdelet, F. Kreuzaler, C. Peterhänsel, S. Schillberg, The expression of a recombinant glycolate dehydrogenase polyprotein in potato (*Solanum tuberosum*) plastids strongly enhances photosynthesis and tuber yield. *Plant Biotechnol. J.* **12**, 734–742 (2014). doi: 10.1111/pbi.12178; pmid: 24605946
36. K. A. Bishop, A. M. Betzelberger, S. P. Long, E. A. Ainsworth, Is there potential to adapt soybean (*Glycine max* Merr.) to future [CO_2]? An analysis of the yield response of 18 genotypes in free-air CO_2 enrichment. *Plant Cell Environ.* **38**, 1765–1774 (2015). doi: 10.1111/pce.12443; pmid: 25211487
37. P. Gallois, P. Marinho, Leaf disk transformation using *Agrobacterium tumefaciens*-expression of heterologous genes in tobacco. *Methods Mol. Biol.* **49**, 39–48 (1995). pmid: 8563823
38. H. Fahnenstich, T. E. Scarpeci, E. M. Valle, U.-I. Flügge, V. G. Maurino, Generation of hydrogen peroxide in chloroplasts of Arabidopsis overexpressing glycolate oxidase as an inducible system to study oxidative stress. *Plant Physiol.* **148**, 719–729 (2008). doi: 10.1104/pp.108.126789; pmid: 18685041
39. K. Głowacka *et al*., An evaluation of new and established methods to determine T-DNA copy number and homozygosity in transgenic plants. *Plant Cell Environ.* **39**, 908–917 (2016). doi: 10.1111/pce.12693; pmid: 26670088
40. K. Oxborough, N. R. Baker, An instrument capable of imaging chlorophyll a fluorescence from intact leaves at very low irradiance and at cellular and subcellular levels of organization. *Plant Cell Environ.* **20**, 1473–1483 (1997). doi: 10.1046/j.1365-3040.1997.d01-42.x
41. G. W. Schmidt, S. K. Delaney, Stable internal reference genes for normalization of real-time RT-PCR in tobacco (*Nicotiana tabacum*) during development and abiotic stress. *Mol. Genet. Genomics* **283**, 233–241 (2010). doi: 10.1007/s00438-010-0511-1; pmid: 20098998
42. S. Wang, L. Yin, J. Mano, K. Tanaka, I. Yin, J. i. Mano, K. Tanaka, Isolation of chloroplast inner and outer envelope

membranes. *Bio Protoc.* **5**, e1405 (2015). doi: 10.21769/BioProtoc.1405
43. J. Kromdijk *et al*., Improving photosynthesis and crop productivity by accelerating recovery from photoprotection. *Science* **354**, 857–861 (2016). doi: 10.1126/science.aai8878; pmid: 27856901
44. A. Brooks, G. D. Farquhar, Effect of temperature on the CO_2/O_2 specificity of ribulose-1,5-bisphosphate carboxylase/oxygenase and the rate of respiration in the light: Estimates from gas-exchange measurements on spinach. *Planta* **165**, 397–406 (1985). doi: 10.1007/BF00392238; pmid: 24241146
45. A. Laisk, Kinetics of photosynthesis and photorespiration in C3 plants. Nauka, Moscow (in Russian) (1977).
46. S. von Caemmerer, J. R. Evans, Temperature responses of mesophyll conductance differ greatly between species. *Plant Cell Environ.* **38**, 629–637 (2015). doi: 10.1111/pce.12449; pmid: 25224884

ACKNOWLEDGMENTS

We thank D. Drag and B. Harbaugh for plant care and management in the greenhouse and field studies; and N. Ferrari, R. Field, G. Lambruschini, J. Ayers, M. Oraweic, R. Devries, R. Gossens, K. Brown, R. Edquilang, and C. Keller for assistance during laboratory and field work. We thank M. Balasubmaranian for tobacco transformation. We thank C. Benjamin for graphic design. We also thank E. Ainsworth, S. Long, B. Walker, and R. Slattery for critical review of the manuscript. **Funding:** This research was supported by Bill and Melinda Gates Foundation grant OPP1172157, titled "RIPE"—Realizing increased photosynthetic efficiency for sustainable increases in crop yield. **Author contributions:** P.F.S, D.R.O, and A.P.C. designed experiments; P.F.S, A.P.C., and H.W.L performed experiments; and P.F.S, D.R.O, A.P.C., and H.W.L analyzed data and wrote the manuscript. **Competing interests:** The authors declare no competing interests **Data materials availability:** The data reported in this paper have been tabulated in the supplementary materials. Plants and constructs reported are available from the University of Illinois for research purposes, subject to the conditions of the Uniform Biological Material Transfer Agreement.

SUPPLEMENTARY MATERIALS

www.sciencemag.org/content/363/6422/eaat9077/suppl/DC1
Figs. S1 to S15
Table S1 to S3
Data S1 to S20

17 April 2018; accepted 20 November 2018
10.1126/science.aat9077

Synthetic glycolate metabolism pathways stimulate crop growth and productivity in the field

Paul F. South, Amanda P. Cavanagh, Helen W. Liu and Donald R. Ort

Science **363** (6422), eaat9077.
DOI: 10.1126/science.aat9077

Fixing photosynthetic inefficiencies

In some of our most useful crops (such as rice and wheat), photosynthesis produces toxic by-products that reduce its efficiency. Photorespiration deals with these by-products, converting them into metabolically useful components, but at the cost of energy lost. South *et al.* constructed a metabolic pathway in transgenic tobacco plants that more efficiently recaptures the unproductive by-products of photosynthesis with less energy lost (see the Perspective by Eisenhut and Weber). In field trials, these transgenic tobacco plants were ~40% more productive than wild-type tobacco plants.

Science, this issue p. eaat9077; see also p. 32